www.adeepakpublishing.com

Tran, Q.-V. et al. (2019): JoSS, Vol. 8, No. 2, pp. 837–847
(Peer-reviewed article available at www.jossonline.com)

www. JoSSonline.com

Development of a Dual-axis Pulsed Plasma Thruster for Nanosatellite Applications

Quang-Vinh Tran, Wee-Seng Lim, and Tran-Duy-Vu Bui

School of Electrical & Electronic Engineering, Nanyang Technological University
Singapore

Kay-Soon Low and Bingyin Kang

National University of Singapore
Singapore

Abstract

This paper reports on the development and evaluation of a dual-axis pulsed plasma thruster (dPPT) for Aoba Velox-III 2U CubeSat at Nanyang Technological University. The mission requirements and thruster design, including electronics and mechanics, are described in detail. A test campaign was conducted to evaluate the dPPT performance in terms of impulse bit I_{bit}, specific impulse I_{sp}, mass bit m_{bit}, discharge voltage, and current of energy storage unit (ESU) response. Finally, experiments were carried out to verify the design consistency with mission requirements. Experiment results were collected to optimize the thruster in the future.

1. Introduction

Since the first nano-satellite (CubeSat) concept was proposed by teams from California Polytechnic State University and Stanford University, the CubeSat sector has grown rapidly as a low-cost solution for access into space for both the space industry and university-level academic research. The absence of a propulsion sub-system, however, limits the lifetime of a CubeSat, due to drag-induced de-orbiting at low earth orbit (LEO). The first ablated pulsed plasma thrusters (PPTs) were successfully employed in space on the Zond-2 and LES-6 CubeSats (Burton and Turchi, 1998). Since then, the PPTs have been used to perform a variety of propulsion tasks not only for drag compensation and formation flying (Ebert, Kowal, and Sloan, 1989; Janson, 1993), but also for station keeping needs (Guman and Nathanson, 1970; Vondra and Thomassen, 1974; Vondra, 1976; LaRocca, 1970), orbit transfer (Akimov et al., 1997), and attitude control (Meckel et al., 1997; Cassady, 1996). The delivered impulse bit of such PPTs ranges from 10 μNs to over 10 mNs, with a wide energy span of 1–700 J (Kamhawi, Arrington, and Pencil, 2005; Kumagai et al., 2003). Hence, the PPTs are a favorable propulsion system in CubeSat applications due to their low energy consumption, simple structure, high specific impulse, no propellant leakage and toxic propellant, low cost, and develop time (Ciaralli et al., 2013).

This article presents the development and test campaign of a dual-axis PPT (dPPT) for a 2U CubeSat named Aoba Velox-III, addressing the mission requirements first. The mechanics and electronics of the dPPT are designed to counteract atmospheric drag

Corresponding Author: Quang-Vinh Tran – Vinh.glory.tran@gmail.com
Publication History: Submitted – 10/26/18; Revision Accepted – 06/25/19; Published – 10/10/19

to prolong the lifespan of the CubeSat by six months in orbit. Finally, a test campaign was conducted to verify that the design was in agreement with requirements of impulse bit, mass bit, specific impulse, propellant consumption, and operation time.

2. Pulsed Plasma Thruster Design

2.1. Mission Requirements

The Aoba-Velox-III (AV3) CubeSat is a joint project of Nanyang Technological University (NTU) and the Kyushu Institute of Technology (Kyutech). Kyutech is responsible for the design of the CubeSat system bus and testing of wireless interconnection. The dual-axis pulsed plasma thruster is the main payload, developed by NTU. The mission of the CubeSat is summarized in Table 1. The AV3 CubeSat will be operated in a circular orbit at an altitude of 400 km and orbital inclination of 51.6°. The size and weight are constrained to 2U and 2.047 kg. Without a propulsion subsystem, the expected lifetime of the AV3 is about three months in orbit, due to drag-induced de-orbiting. To extend the lifespan of the AV3 to six months, an ablated PPT is employed to compensate the drag at an altitude that meets the requirements in terms of power, mass, volume, total impulse, and specific impulse. Hence, the correlation between the fuel consumption and the satellite lifetime extension are analyzed in simulations, shown in Table 2. At an altitude of 400 km and drag coefficient of 2.2, the dPPT must provide at least 355,000 shots to extend the mission lifespan to 6.04 months. Assuming a minimum specific impulse I_{sp} of 500 s, the required propellant is 2.84 g and expected total impulse of 13.93 Ns. The structure budget proposed by Kyutech constrains the maximum size of the dPPT to 83 x 83 x 90 mm of width, height, and length, with a weight that does not exceed 500 g. The average input power is chosen to be 2.25 W, well suited for the solar panels of the 2U CubeSat. The dPPT requirements are depicted in Table 3.

Table 1. Aoba-Velox-III CubeSat Mission

Parameter	Value
Orbit	Altitude: 400 km
	Orbital inclination: 51.6°
Size / weight	2U / 2.047 kg
Mission duration with assisted dPPT	6 months

2.2. Thruster's Geometrical Selection

The propellant feeding mechanism, shape of electrodes, and energy shot of the dPPT were selected based on the mission requirements and performance. First, the propellant feeding mechanism was considered, to overcome the constraint of the dPPT dimension. The main task of the dPPT is atmospheric drag compensation in LEO, whereas the sub-task is attitude control in the future. Hence, the dPPT is designed using a breech-fed configuration for angular rate measurement and a side-fed configuration for drag compensation. The breech-fed configuration is mounted un derneath the side-fed one and shares the same as an ESU to minimize the dPPT dimension as shown in Figure 1.

Thrust performance is expressed by impulse bit I_{bit}. To maximize thrust performance, the inductance variation per unit length, i.e., the inductance gradient L', should be maximized by the design of electrodes shape and aspect ratio *h/w* between electrodes separation *h* and width *w* (Guman, Vondra, and Thomasson, 1970; Palumbo and Guman, 1976; Yuan-Zhu, 1984; Arrington, Haag, and Pencil, 1997). The impulse bit of rectangular parallel electrodes can be calculated by Eqn. (1) below, in terms of the inductance gradient *L'* and the discharge current *i*, where the inductance

Table 2. Lifetime Extension Summary

Satellite lifetime (months)	Extension (months)	ΔV budget (m/s)	Fuel mass budget (g)	No. of shots
5.28	2.18	6.47	2.27	283,750
6.04	2.9	6.81	2.84	355,000
6.68	3.54	8.18	3.41	426,250
12.48	9.34	16.35	6.82	852,500

Table 3. Requirements of the dPPT for Drag Compensation

Requirement	Value
Maximum volume	83 x 83 x 90 mm
Maximum weight	< 500 g
Maximum propellant mass	10 g
Total impulse	13.93 Ns
Minimum I_{sp}	500 s
Average input power	2.25 W

gradient *L'* is determined in units of μH/m using Eqn. (2) and expressed in terms of the electrode separation *h*, elec trode width *w*, and electrode thickness *d* (Burton and Turchi, 1998; Pottinger, Krejci, and Scharlemann, 2011). Assuming that the PPT is modeled as an underdamped RLC circuit, the discharge current waveform is depicted in Figure 2. Circuit equivalent inductance *L*, resistance *R*, and discharge current *i* are determined by Eqns. (3)–(5) in terms of known system capacitance *C*, peak discharge current I_1, minimum discharge current I_2, and period of the first discharge current cycle *T*, respectively (Jackson, 1998).

According to Pottinger, Krejci, and Scharlemann (2011), increasing to a higher aspect ratio *h/w* of the electrodes can produce a higher impulse bit for the same input energy density. However, if the aspect ratio is too high, the significant non-uniformities increase in the electromagnetic field, hence reducing acceleration process efficiency (Jahn, 1968). Recently, many studies on tongue-shaped electrodes have been carried out to improve the inductance gradient (Vondra, and Thomasson, 1970; Palumbo and Guman, 1976; Yuan-Zhu, 1984; Arrington, Haag, and Pencil, 1997; Pottinger, Krejci, and Scharlemann, 2008). These efforts have shown that the flared tongue-shaped electrodes typically double the impulse bit produced in comparison with the rectangular parallel electrodes, because the maximum inductance gradient of the flared geometries is approximately twice of the parallel ones. However, the inductance gradient of flared tongue geometries cannot be determined analytically due to a limitation of zero electrodes width and thickness. As a solution, the geometry is divided into sections of equal length with sequentially decreasing width and thickness. Then, the inductance gradient is calculated for each section and

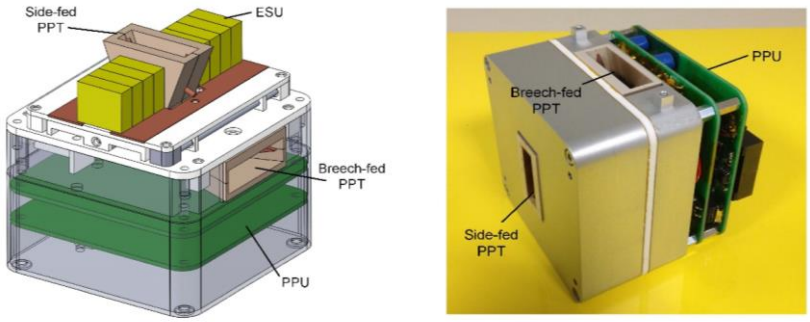

Figure 1. Proposed dPPT configuration: a) CAD dPPT design and b) actual dPPT.

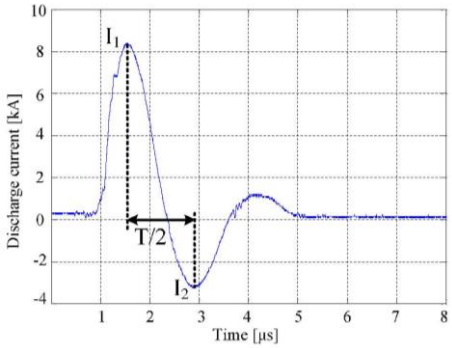

Figure 2. Discharge current pattern.

the average values are used to determine the impulse bit. The analysis motivates the use of PPT electrodes as 200 flared angle tongued-shape with corresponding aspect ratio *h/w* of 1.5 and 2 for breech-fed and side-fed configuration, respectively. Copper-tungsten alloy serves as electrode material due to its advantageous mechanical and thermal properties, low parasitic inductance and resistance, and reduced erosion rate (Clark et al., 2011). Figure 3 shows a typical configuration of side-fed PPT with flared angle, tongued-shape electrodes, where *h*, *w*, and *d* are separation, width, and thickness of the electrodes, respectively.

$$I_{bit} = \frac{L'}{2}\int_0^t i^2 dt \quad (1)$$

$$L' = 0.6 + 0.4ln\left(\frac{h}{w+d}\right) \quad (2)$$

$$i = -\frac{V_o}{L}\frac{1}{\sqrt{\frac{1}{LC}-\frac{R^2}{4L^2}}}exp\left(-\frac{R}{2L}t\right)sin\left(t\sqrt{\frac{1}{LC}-\frac{R^2}{4L^2}}\right) \quad (3)$$

$$R = \frac{2L}{T}ln\left(\frac{I_1}{I_2}\right) \quad (4)$$

$$L = \frac{T^2}{4\pi^2 C} \quad (5)$$

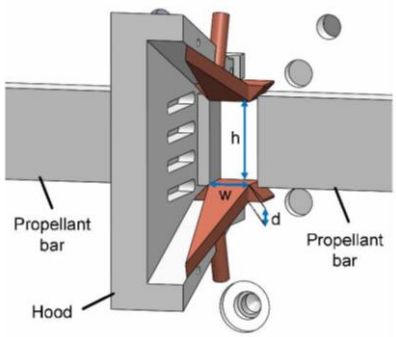

Figure 3. Typical side-fed PPT configuration with flared angle, tongued-shape electrodes.

Besides the electrode geometry, the ratio of discharge energy to propellant area *E/A* affects thrust performance in terms of specific impulse I_{sp} and propellant consumption. Many studies have proven that the higher *E/A* ratio produced the higher specific impulse I_{sp} (Clark et al., 2011; Gessini and Paccani, 2001; Guman, 1975; Palumbo and Guman, 1972; Gessini et al., 2002). Figure 4 shows the curve of semi-empirical relations between the specific impulse with the *E/A* ratio predicted by Gessini-Paccani and Guman (Clark et al., 2011; Gessini and Paccani, 2001; Guman, 1975). To compensate for the aforementioned drag-induced de-orbiting, the specific impulse of the side-fed PPT should not fall below a certain threshold, to complete the mission. Hence, the *E/A* ratio has been chosen about 2 J/cm^2 based on what is given by the Guman curve to produce a minimum specific impulse I_{sp} of 500 s that meets the requirement of dPPT shown in Table 3. The geometrical design of the thruster is summarized in Table 4.

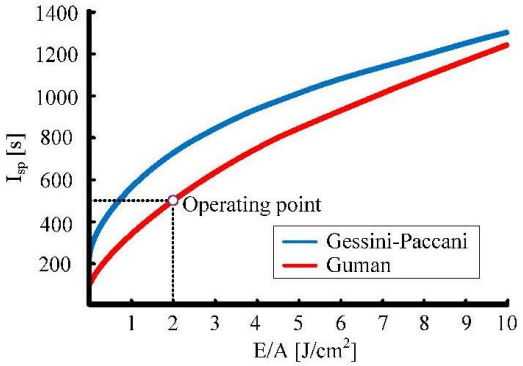

Figure 4. Semi-empirical specific impulse versus E/A ratio.

Table 4. Summary of Geometrical Thruster Design

Parameter	Specification	
	Breech-fed configuration	**Side-fed configuration**
Capacitance of ESU	2 µF (08 x 0.25 µF capacitor 7565R254k202k)	
Nominal ESU voltage	1500 V	
Maximum igniter voltage	6400 V	
Discharge energy	2.25 J	
Electrode shape	200 flared, tongued shape	
Aspect ratio h/w	1.5	2

2.3. Electronics Design

The block diagram of the electronic design of the dPPT is shown in Figure 5. The dPPT consists of a breech-fed and a side-fed PPT that share an ESU, to minimize volume and cost. The ESU is a capacitor bank including eight 0.25 µF high-frequency pulsed

energy capacitors rated up to 2000 V from Novacap company that provides a total nominal bank capacitance of 2.0 μF. The ESU is charged up to 1500 V to store an amount energy of 2.25 J. The power processing unit (PPU) that powers the dPPT comprises a capacitor charged power supply, an igniter power supply, a synchronous control circuit, and a sensing circuit. The capacitor charged power supply is a flyback converter using an LT3750 controller (see Analog Device: LT3750), to boost the 5 V from the CubeSat power bus to 1500 V for charging the ESU. The ESU is connected to both pairs of electrodes of the breech-fed and the side-fed PPT. Two in-house coaxial igniters were developed to trigger the operation of the dPPT. A copper rod serves as the positive electrode of the igniter. The power supply of the igniter comprises a pair of push-pull resonant inverter and Cockcroft–Walton (CW) voltage multiplier to supply a maximum voltage of 6400 V for two coaxial igniters (Tuan, Chang, and Song, 2007; Lamantia, Maranesi, and Radrizzani, 1990). The igniter generates a small spark between the copper rod and the negative electrode of the dPPT. This results in a current path to trigger the ESU discharging its energy at a firing rate of 1 Hz. The high discharged current of ESU ablates and ionizes the Teflon propellant to form a desirable plasma and thrust. The control circuit aims to synchronize the operation of the capacitor charged power supply and the igniter power supply. The igniter can only be activated after the ESU is charged to the designated voltage level. An on-board computer (OBC) sends a command to the synchronous control circuit to independently trigger Igniter 1 or Igniter 2 to fire the corresponding breech-fed and side-fed PPT, respectively. Regarding telemetry, a sensing circuit is designed to count the firing number of the ESU and transmit to the OBC for recording and computing angular rate produced by the dPPT. The used transformers in the capacitor charged and the igniter power supply are isolated; therefore, the electronics board can be electrically isolated from the thruster electrodes. This design allows keeping the thruster afloat, which avoids noise and ground shifts during operation. The PPU is 82 x 82 x 37 mm in size, and it interfaces with a satellite bus via a Dsub-9 connector. The actual PPU image is shown in Figure 6.

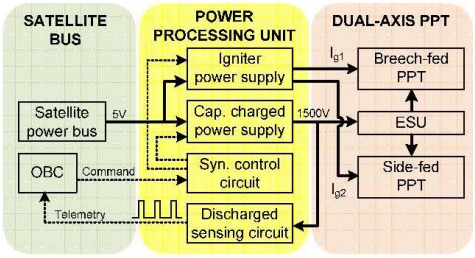

Figure 5. Electronics design and interface of the proposed dPPT.

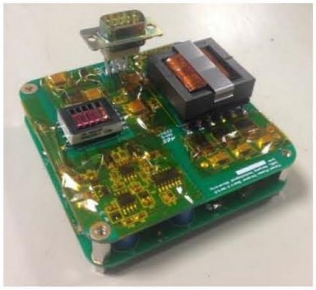

Figure 6. Power processing unit of the proposed dPPT.

3. Experiment Results

3.1. Experiment Setup

An experiment was conducted to verify that the dPPT performance satisfies the mission requirements. The dPPT, configured as shown in Figure 7, was tested in a horizontal, stainless-steel, cylinder-type vacuum chamber with a volume of 0.28 m^3. The vacuum level was maintained at 10^{-5} mbar throughout the test, using a Pfeiffer pumping system that consisted of a duo line-based pump and a HiPace 400 molecular pump with a speed of 355 l/s. The PPU and dPPT were placed inside the vacuum chamber and powered by a 5V/10A power supply (PWS). The ESU voltage was measured by a high voltage differential probe. A Rogowski coil was used to gauge the ESU discharged current. The thrust impulse bit generated by the dPPT was investigated by a torsional micro-newton thrust stand that was developed in-house. These measured signals were displayed on an Instek oscilloscope put outside the vacuum chamber. For telemetry and command activities, an OBC was designed to send a

command to PPU via two general-purpose I/O ports to control the dPPT's igniters. Meanwhile, a discharged sensing circuit sensed the ESU voltage and converted it to a square-wave digital signal for counting the number of firings. This signal was transmitted to the OBC through an external interrupt. A personal computer interfaced to the OBC and thrust stand via serial communication to record the firing number and calculate impulse bit, respectively.

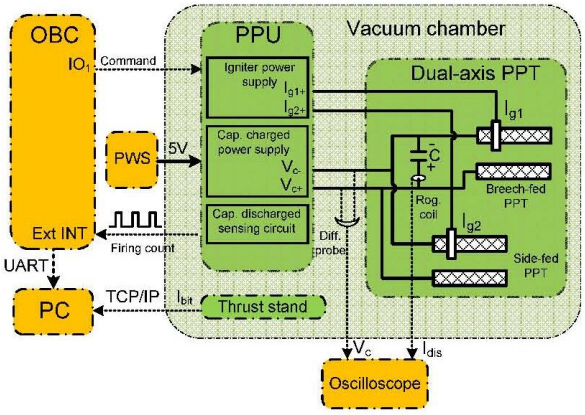

Figure 7 Experimental setup of the dPPT.

3.2. Experiment Results

The test campaign aimed to investigate the performance of the dPPT and gather the experiment data for optimizing the design in the future. The discharged voltage and current of the breech-fed and side-fed PPT were measured by high voltage differential probe and Rogowski coil, shown in Figure 8. As mentioned earlier, the 2.0 µF capacitor bank of ESU was charged to 1.5 kV to store an amount of energy of 2.25 J. The energy was released by triggering of the corresponding igniter to form a peak discharged current of 4.2 kA and 5.92 kA for the breech-fed and the side-fed PPT, respectively. The discharge current oscillated in the manner of a damped sinusoidal waveform for a time interval of 4.0 µs and 2.57 µs as the external RLC circuit impedances exceed the discharge impedance. The waveform of the discharge currents is complied with in the aforementioned analysis, in comparison with Figure 2 and Eqn. (3). It was noted that reversing the current would reduce the capacitor lifetime and the effectiveness of the ablation and acceleration processes. The current reversal also increased electrode sheath losses and heat transfer. An optimum pulse shape is the non-reversing unipolar pulse (Burton and Turchi, 1998). Nevertheless, the current waveform was completely damped after the first oscillation cycle. It can be concluded that the system is not too far away from the optimal critical damping condition. Moreover, for telemetry activities, a circuit sensed the falling edge of ESU discharged voltage and generated a rectangular pulse to inform to the OBC once one discharge occurs, as shown in the second trace of Figure 9.

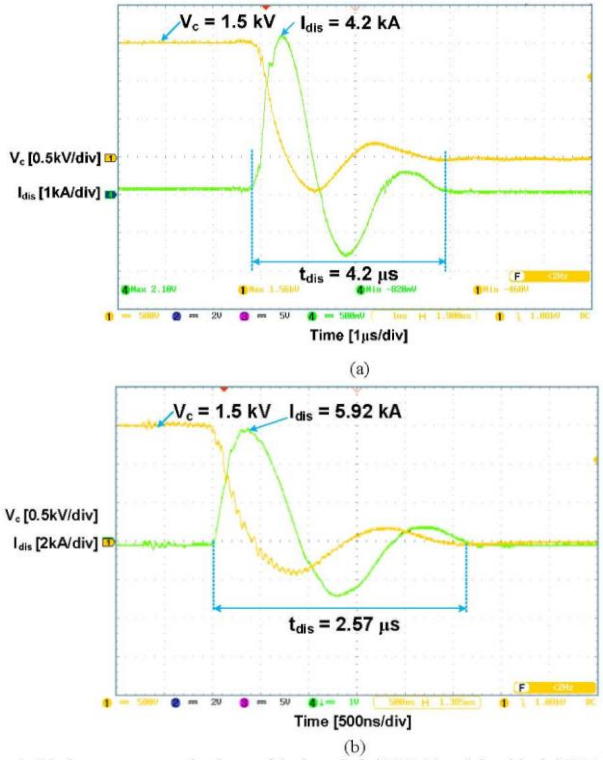

Figure 8. Discharge current and voltage of the breech-fed PPT (a) and the side-fed PPT (b).

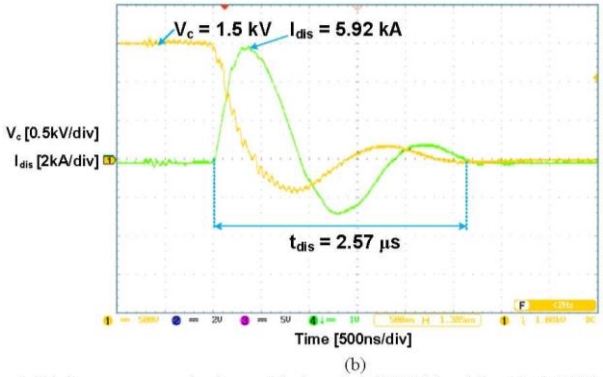

Figure 9. Firing count signal of the proposed dPPT.

The performance of the proposed dPPT was tested in a vacuum chamber at the Satellite Research Centre, Nanyang Technological University. Figures 10(a) and (b) show a uniform plasma plume of the breech-fed (off-axis) and the side-fed PPT (primary), respectively. The propellant bar at different circumstance of the side-fed PPT is shown in Figure 11. The full propellant bar of 10 g at the initial condition is shown in Figure 11(a). After 30,000 shots, the propellant surface was investigated. It can be noted that the whole surface of the propellant bar was consumed to form the uniform plasma as presented in Figure 11(b). The test has been conducted continuously up to 300,000 shots. Hence, almost one third propellant bar was consumed as shown in Figure 11(c). The target of this campaign is an accumulation of 1,000,000 shots to consume all of the propellant. However, the ablation on the left-side propellant bar was not evenly consumed this time. This was caused by the asymmetry of the electrodes, the left-side bar being closer to the igniter than the right-side one.

3.3. Impulse Bit, Mass Bit and Specific Impulse Measurement

Impulse bit I_{bit}, specific impulse $I_{sp,}$ and mass bit m_{bit} were investigated to assess the design of the dPPT and conformance with the aforementioned mission requirements. A micro-Newton thrust stand developed in-house (shown in Figure 12) was used to measure the impulse bit (Gamero, 2003; Koizumi, Komurasaki, and Arakawa, 2004). The torsional arm length is pre-defined at 0.5m. The pivot is Riverhawk 6012-400 flexural. This stainless-steel frictionless pivot has a torsional spring rate of 0.0434Nm/^{o} and displays significant advantages over conventional bearings: it is lubricant free, vacuum compatible, and resistant to thermal stress. The linear displacement sensor is an optical sensor (ILD 2300-2, Micro Epsilon). This sensor operates based on the principle of triangulation, non-contact, and non-intrusive nature, and has a measuring range of 2 mm with 30 nm resolution. Moreover, a passive magnetic damper was used to dissipate the kinetic energy of the stand after perturbation, to bring the stand to as rest and prepare it for the next measurement. The characteristics of the thrust stand are summarized in detail in Table 5.

The stand was first calibrated using an electrostatic calibrator (Pancotti, Gilpin, and Hilario, 2012). Thereafter, ten single shot measurements were taken. A typical single shot produced a nominal displacement value of 25.3μm with standard deviation of 0.5μm. Using the calibration curve, the impulse bit is evaluated at 39.1μNs and 22.4 μNs with an error budget of ±1.3μNs for the side-fed PPT and the breech-fed PPT, respectively. The calibration curve

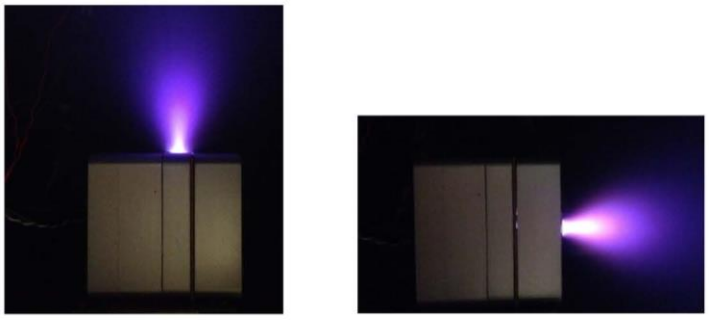

(a) (b)

Figure 10. Plasma plume of the breech-fed PPT (a) and the side-fed PPT (b).

(a) (b) (c)

Figure 11. Propellant bar at initial condition (a), after 30,000 shots condition (b), and after 300,000 shots condition (c).

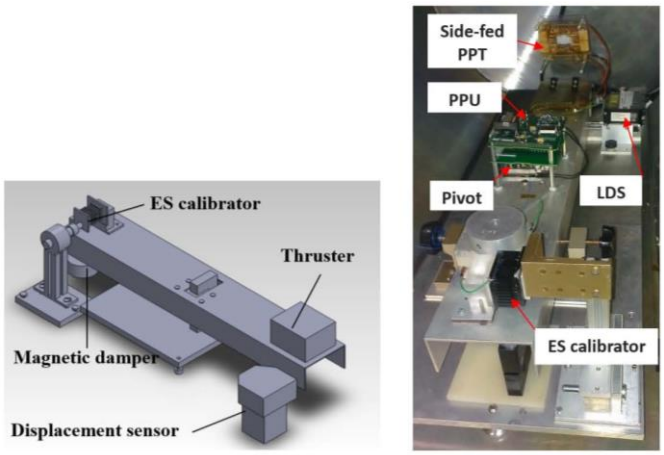

Figure 12. Schematic of the thrust stand (a) and the actual setup in vacuum chamber (b).

Table 5. Characteristics of the Stand

Parameters	Specification
Natural Frequency	0.819 Hz
Sensitivity	4.56 μN/μm
Noise	0.12 μm
Zero drift	0.15 nN/s
Resolution	0.55 μN

and a typical thrust stand response to PPT single shot is shown in Figures 13 and 14, respectively.

The specific impulse of the propulsion system I_{sp} is the amount of impulse delivered to the spacecraft per unit propellant consumed. The I_{sp} of the dPPT can be indirectly calculated once its impulse bit I_{bit} and mass bit m_{bit} are known by using Eqn. (6). The I_{bit} and m_{bit} are described as the impulse delivered and

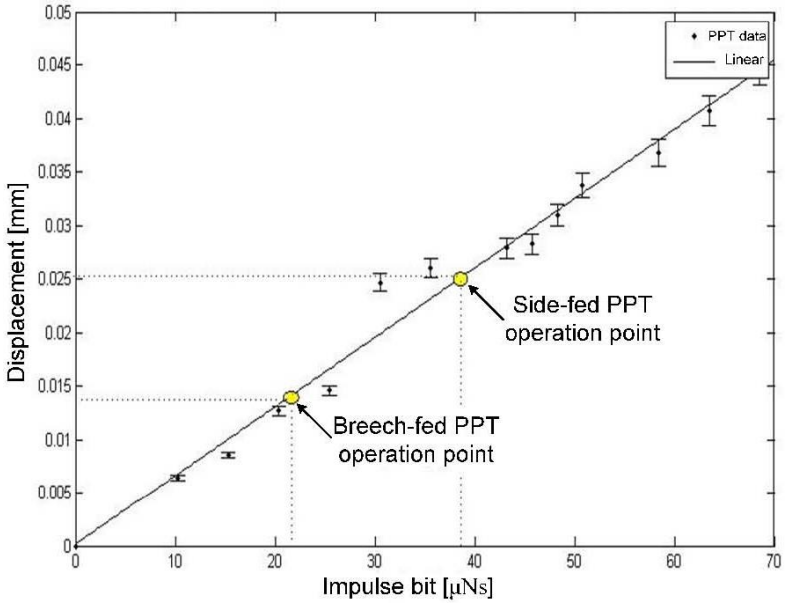

Figure 13. Thrust stand calibration curve.

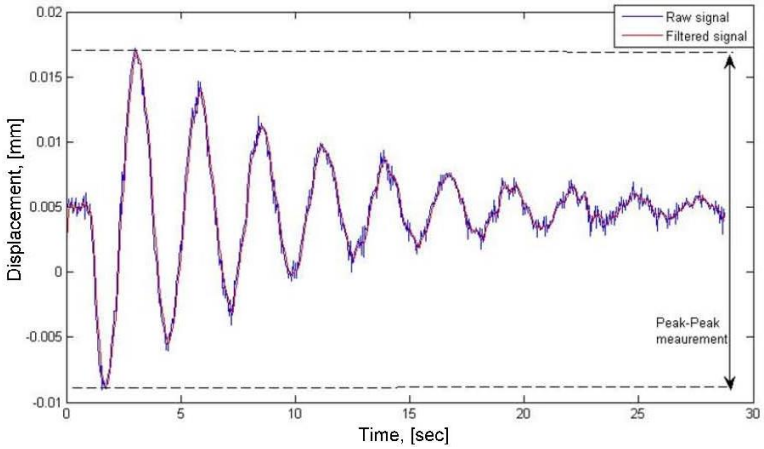

Figure 14. Typical dPPT single shot thrust stand response.

the measure of propellant consumption per shot, respectively. Hence, the m_{bit} can be physically calculated by measuring the deviation of the propellant mass before and after N number of firing and then divide by the number of firing N, as in the following Eqn. (7):

$$I_{sp} = \frac{I_{bit}}{m_{bit} g_0} \tag{6}$$

$$m_{bit} = (M_i - M_f)/N \tag{7}$$

where g_0 is the standard gravitational acceleration g_0 = 9.81 m/s^2, and M_i and M_f are propellant masses before and after N number of firing, respectively.

In practice, the propellant mass was measured by using a high precision balance. The averaged mass bit consumption m_{bit} of the side-fed and the breech-fed PPT were 7.34 µg and 4.34 µg. This resulted in a number of specific impulses of 543 s and 525 s for the side-fed and the breech-fed PPT, respectively. It was noted that the obtained specific impulse of the proposed dPPT has met the required one to fulfill the CubeSat mission. The target and performance achievements of the dPPT are summarized in Table 6. It can be seen that the obtainable performance is fully in agreement with the target.

4. Conclusion

This article has presented the development of a dual-axis pulsed plasma thruster for a 2U CubeSat at Nanyang Technological University. The thruster design, including mechanical, electrical components, and mission analysis, was described in detail. The electrodes were selected as 20° flared angle tongued-

Table 6. Target and Achieved Performance of the dPPT

Parameter	**Target**	**Achieved performance**	
		Breech-fed configuration	**Side-fed configuration**
Capacitance of ESU	2 Mf	2 µF	
Nominal ESU voltage	1500 V	1500 V	
Pulse rate	1 Hz	1 Hz	
Average power	2.25 W	2.25 W	
Dry weight	< 500 g	490 g	
Size	83 x 83 x 90 mm	83 x 83 x 88 mm	
Peak discharge current		4200 A	5920 A
Impulse bit		22.4 ±1.3µNs	39.1 ±1.3µNs
Mass bit		4.35 µg	7.34 µg
Specific impulse	500 s	525 s	543 s
Total impulse for drag compensation	13.93 Ns	51.50 Ns	53.26 Ns

shape with aspect ratio *h/w* of 1.5 and 2 for breech-fed and side-fed configuration, respectively. The PPU supplied a voltage of 1500 V and 6400 V to the ESU and the relevant igniters. The performance of the dPPT in terms of impulse bit I_{bit}, specific impulse I_{sp}, mass bit m_{bit}, discharge voltage, and current of energy storage unit response was evaluated in a test campaign. A micro-Newton thrust stand that was developed in-house determined the impulse bit of the side-fed and the breech-fed PPT as 39.1 µNs and 22.4 µNs with an error budget of ± 1.3 µNs, respectively. This resulted in a number of specific impulses of 543 s and 525 s. Long term operation of one million shots has been conducted to investigate the dPPT lifetime, and has provided data for optimization of the dPPT in future research. The performance of the dPPT meets the mission requirements in terms of power, mass, volume, total impulse, and specific impulse.

References

Akimov, V. et al. (1997): Analysis of PPT Potentialities in Solving the Satellite Orbit Control Tasks, in *Proc. 25th Int. Elec. Prop. Conf.*, Aug. 24–28, Cleveland, OH US, pp. 906–910.

Analog Device: LT3750 – Capacitor Charger Controller: Available at: https://www.analog.com/en/products/lt3750.html?gclid=CjwKCAjwtYXmBRAOEiwAYsyl3KJoM_nXp_jWuDchC0bzVnk55ENdNMaFieFtNjczSJWpCX7H-Ie3VhoCyiEQAvD_BwE#product-overview.

Arrington, A. A., Haag, T. W., and Pencil, E. J. (1997): A Performance Comparison of Pulsed Plasma Thruster Electrode Configurations, in *Proc. 25th Int. Elec. Prop. Conf.*, Aug. 24–28, Cleveland, OH US, pp. 1–12.

Burton, R. L. and Turchi, P. J. (1998): Pulsed Plasma Thruster. *J. of Propulsion and Power*, Vol. 14 (5), pp. 716–735.

Cassady, R. J. et al. (1996): Pulsed Plasma Thruster Systems for Spacecraft Attitude Control, in *Proc. 10th Ann. AIAA/USU Conf. on Small Satellites*, Sept. 16–19, Logan, UT US, pp. 26–37.

Ciaralli, S. et al. (2013): PPTCUP Lifetime Test Results, in *Proc. 33rd Int. Elec. Prop. Conf.*, Oct. 6–10, Washington DC, pp. 1–15.

Clark, C. et al. (2011): An Off the Shelf Electric Propulsion System for CubeSats, in *Proc. 25th Ann. AIAA/USU Conf. on Small Satellites*, pp 1–13.

Ebert, W. L., Kowal, S. J., and Sloan, R. F. (1989): Operational Nova Spacecraft Teflon Pulsed Plasma Thruster System, in *Proc. 25th Am. Soc. of Mech. Eng. Jt. Prop. Conf.*, July 12–16, Monterey, CA US, pp. 1–11.

Gamero-Castano, M. (2003): A Torsional Balance for the Characterization of MicroNewton Thrusters. *Rev. of Scientific Instruments*, Vol. 74 (10), pp. 4509–4514.

Gessini, P. et al. (2002): Propulsion System Optimization for Satellite Formation Flying, in *Proc. 4th Int. Workshop on Satellite Constellations and Formation Flying, INPE*, Mar. 1–3, São José dos Campos, Brazil, pp. 1–5.

Gessini, P. and Paccani, G. (2001): Ablative Pulsed Plasma Thruster System Optimization for Microsatellites, in *Proc. 27th Int. Elec. Prop. Conf.*, Oct. 15–19, Pasadena, CA US, pp. 1–13.

Guman, W. J. (1975): Designing Solid Propellant Pulsed Plasma Thruster, in *Proc. AIAA-1975-410, 11th Elec. Prop. Conf.*, Mar. 19–21, New Orleans, LA US, pp. 1–8.

Guman, W. J. and Nathanson, D. M. (1970): Pulsed Plasma Micro-Thruster Propulsion System for Synchronous Orbit Satellite. *J. of Spacecraft and Rockets*, Vol. 7 (4), pp. 409–415.

Guman, W. J., Vondra, R. J., and Thomassen, K. (1970): Pulsed Plasma Propulsion System Studies, in *Proc. 8th Elec. Prop. Conf.*, Aug. 31–Sept. 2, Standfort, CA US, pp. 1–11.

Jackson, J. D. (1998): *Classical Electrodynamics*, 3rd ed., Wiley: New York, NY.

Jahn, R. (1968): *Physical of Electric Propulsion*, McGraw-Hill: New York, NY.

Janson, S. W. (1993): The On-Orbit Role of Electric Propulsion, in *Proc. 29th Jt. Prop. Conf. and Exhibit*, June 28–30, Monterey, CA US, pp. 1–13.

Kamhawi, H., Arrington, L., and Pencil, E. (2005): Performance Evaluation of a High Energy Pulsed Plasma Thruster, in *Proc. 29th Int. Elec. Prop.*

Conf., Oct. 31–Nov. 4, Princeton Univ., NJ US, pp. 1–18.

Koizumi, H., Komurasaki, K., and Arakawa, Y. (2004): Development of Thrust Stand for Low Impulse Measurement from Microthrusters. *Rev. of Scientific Instruments*, Vol. 75, pp. 3185–3190.

Kumagai, N. et al. (2003): Research and Development Status of Low Power Pulsed Plasma Thruster System for μ-Lab Sat II, in *Proc. 28th Int. Elec. Prop. Conf.*, Mar. 17–21, Toulouse, FR, pp. 1–11.

Lamantia, A., Maranesi, P., and Radrizzani, L. (1990): The Dynamics of the Cockcroft-Walton Voltage Multiplier, in *Proc. Power Electronics Specialists Conf., PESC '90 Rec., 21st Ann. IEEE*, June 11–14, TX US, pp.48–49.

LaRocca, A. V. (1970): Pulsed Plasma Thruster System for Attitude and Station Control of Spacecraft. *First Western Space Conf.*, pp. 688–702.

Meckel, N. J. et al. (1997): Investigation of Pulsed Plasma Thrusters for Spacecraft Attitude Control, in *Proc. 25th Int. Elec. Prop. Conf.*, Aug. 24–28, Cleveland, OH US, pp. 813–820.

Palumbo, D. J. and Guman, W. J. (1972): Continuing Development of the Short Pulsed Ablative Space Propulsion System, in *Proc. 8th Jt. Prop. Conf.*, Nov. 29–Dec., New Orleans, LA US, pp. 1–7.

Palumbo, D. J. and Guman, W. J. (1976): Effects of Propellant and Electrode Geometry on Pulsed Ablative Plasma Thruster Performance. *J. of Spacecraft and Rockets*, Vol. 13 (3).

Pancotti, A. P., Gilpin, M. and Hilario, M. S. (2012): Comparison of Electrostatic Fins with Piezoelectric Impact Hammer Techniques to Extend Impulse Calibration Range of a Torsional Thrust Stand. *Rev. of Scientific Instr.*, Vol. 83 (3), pp. 035109-1 – 035109-8.

Pottinger, S. J., Krejci, D., and Scharlemann, C. A. (2008): Development of a PPT for CubeSat applications, in *Proc 44th AIAA/ASME/SAE/ASEE Jt. Prop. Conf.*, July 21–23, Hartford, CT US, pp. 1–13.

Pottinger, S. J., Krejci, D., and Scharlemann, C. A. (2011): Pulsed Plasma Thruster Performance for Miniaturized Electrode Configurations and Low Energy Operation. *Acta Astronautica*, Vol. 68, pp. 1996–2004.

Tuan, Y., Chang, L., and Song, P. (2007): A New LCL-Resonant Push-Pull DC-DC Converter for Inverter Applications, in *Proc. Power Eng., 2007 Large Engineering Systems Conf.*, Oct. 10–12, Montreal, CA, pp. 261–264.

Vondra, R. J. (1976): The MIT Lincoln Laboratory Pulsed Plasma Thruster – A Final Report on the LES-8/9 Pulsed Plasma Thruster, in *Proc. 12th Int. Elec. Prop. Conf.*, Nov. 14–17, Key Biscayne, FL US, pp. 1–9.

Vondra, R. J., and Thomassen, K. I. (1974): Flight Qualified Pulsed Electric Thruster for Satellite Control. *J. of Spacecraft and Rockets*, Vol. 11 (9), pp. 613–617.

Yuan-Zhu, K. (1984): Effects of Propellant Geometry on PPT Performance, in *Proc. 17th Int. Elec. Prop. Conf.*, Tokyo, JP, pp. 84–94.